Article

Biotin-Tagged Polysaccharide Vesicular Nanocarriers for Receptor-Mediated Anticancer Drug Delivery in Cancer Cells

Nilesh Umakant Deshpande, and Manickam Jayakannan

Biomacromolecules, **Just Accepted Manuscript** • DOI: 10.1021/acs.biomac.8b00833 • Publication Date (Web): 15 Jun 2018

Biotin-Tagged Polysaccharide Vesicular Nanocarriers for Receptor-Mediated Anticancer Drug Delivery in Cancer Cells

Nilesh Umakant Deshpande and Manickam Jayakannan*

Department of Chemistry
Indian Institute of Science Education and Research (IISER) Pune
Dr. Homi Bhabha Road
Pune 411008, Maharashtra, India

*Corresponding Author: jayakannan@iiserpune.ac.in

Keywords: Receptor-mediated endocytosis, Polysaccharide vesicles, Multi-stimuli-responsiveness, GSH redox stimuli, Enzymatic-biodegradation, Drug delivery.

Abstract

Biotin-conjugated multi-stimuli-responsive polysaccharide vesicular nanocarriers are designed and developed, for the first time, to accomplish receptor-mediated endocytosis in cancer cells and to deliver anticancer drugs at the intracellular compartments. For this purpose, a new renewable hydrophobic unit was custom designed with redox-degradable disulphide and enzyme-biodegradable aliphatic ester chemical linkages and it was conjugated along with biotin on the dextran backbone. The dextran derivative self-assembled into nanovesicles of < 200 nm in size which were characterized by dynamic and static light scattering, electron and atomic force microscopes. Avidin-HABA assay established the high affinity of biotin-tagged dextran vesicles towards membrane-receptors up to 25 nM concentration. Doxorubicin-hydrochloride (DOX.HCl) loaded dextran vesicles exhibited stable formulation in PBS and FBS. Redox-degradation by glutathione (GSH) showed 60 % drug release whereas lysosomal esterase enzyme enabled > 98 % drug release in 12 h. Confocal microscope and flow cytometry assisted time-dependent cellular uptake studies revealed that the biotin-receptor over expressed cervical cancer cells (HeLa) exhibited larger

drug accumulation through receptor-assisted endocytosis process. This process enabled the delivery of higher amount of DOX and significantly enhanced the killing in cancer cells (HeLa) compared to wild-type mouse embryonic fibroblast cells (WT-MEF, normal cells). Control experiments such as biotin pre-treatment in cancer cells and energy-suppressed cellular uptake at 4 °C further supported the occurrence of receptor-mediated endocytosis by the biotin-tagged polymer vesicles. This report provides first insights into the targeted polysaccharide vesicle platform, and the proof-of-concept is successfully demonstrated in biotin receptors over expressed cervical cancer cells.

Introduction

Receptor-mediated endocytosis of nano-carriers is emerging as one of the important approaches for targeted delivery of anticancer drugs or genes to cancer tissues under physiological conditions.[1-4] Cancer cells are over expressed by large number of signalling receptors for metastasis and also enriching the nutrient supply to the fast and uncontrolled cell growth. [5-7] These receptors exhibit high binding affinity towards targeting ligands such as biotin (vitamin B7),[8-9] folic acid[10-13] and RGD peptide,[14] tranSerrin[15] etc. Nano-assemblies tagged with these targeting ligands enhance the delivery of payload at the cancer tissue site through receptor-ligand interaction.[3] Biotin is one of the excellent targeting ligands for streptavidin-type membrane proteins (avidin class of proteins) at the cell surface with high association constant[16] in the range of 10^{13} to10^{15} M^{-1}. Various cancer cells such as cervical, breast, lung, and ovarian are over expressed with biotin receptors.[17] Biotin-conjugated nano-assemblies from small molecules,[18] block copolymers,[19-21] dendrimers,[12] gold nanoparticles,[22] and carbon nano-tubes,[23] etc were explored for delivering chemotherapeutic agents. The polymer nano-carriers are particularly important since they have unique capability to passive selectively target the cancer tissue via enhanced permeability and retention effect (EPR).[24-25] Thus, the receptor-mediated endocytosis in macromolecular nano-carriers is an appropriate choice for both active and passive selectively targeting the cancer tissues. Bio-resource based polymer nano-carriers have recently gained significant importance in bio-medical field.[26-27] Polysaccharide nano-carriers are unique bio-resource systems due to their excellent biocompatibility associated with structural diversity,[28-31] and also possess sugar-type macromolecular backbone for enhanced internalisation via like-like interaction with lectins (carbohydrate-binding proteins) at the cell membrane.[32-34] Polysaccharide micelles,[35]

nanoparticles,[36]capsules,[37] hydrogels,[38-40] and polymersomes (or vesicles)[28-31] were reported for drug and gene delivery. Among these nano-carriers; polysaccharide nanovesicles are very unique for delivering both water soluble and water insoluble anticancer drugs from single nano-carrier.[41] Earlier dextran vesicles using stearyl chains as hydrophobic unit and folate as targeting ligand were reported for delivering doxorubicin.[42-43] From our group, new classes of enzyme and pH responsive polysaccharide vesicles were reported based on dextran and renewable resource hydrophobic units from cashew nut shell liquid.[41, 44-45] Uptake studies using caveolae (+) plus and caveolae (-) nul cells revealed that the dextran vesicles were significantly taken up by the caveolae (-) nul type cells that resembled the membrane architectures of breast cancer cells.[46] Carboxylic functional dextran vesicles were designed to administrate three different antagonistic drugs like doxorubicin (DOX), camptothecin, and cisplatin together for synergistic combination therapy.[47] Polymersomes or polymer vesicles are one of the most important multipurpose nano-carriers for drug delivery; however, the concept of targeted polysaccharide vesicle is not fully explored for better treatment efficiencies in cancer. Despite biotin being known as excellent targeting ligand to cancer cells; there is no report on biotin-tagged polysaccharide vesicles in the literature. The lack of the non-availability of structural motifs for maintaining appropriate hydrophobic-hydrophilic balance is one of the reasons with respect to the difficulty in producing biotin-tagged polysaccharide vesicular assemblies. The present work is the first example to address this important idea and the proof-of-concept is successfully demonstrated in cancer cell lines. Here, we report biotin-tagged and multi-stimuli-responsive polysaccharide vesicles based on dextran backbone and renewable resource hydrophobic unit. The receptor-mediated endocytosis concept was successfully demonstrated *in vitro* by carefully designed time-dependent cellular uptake studies in cancer cells. This new concept is shown in figure 1.

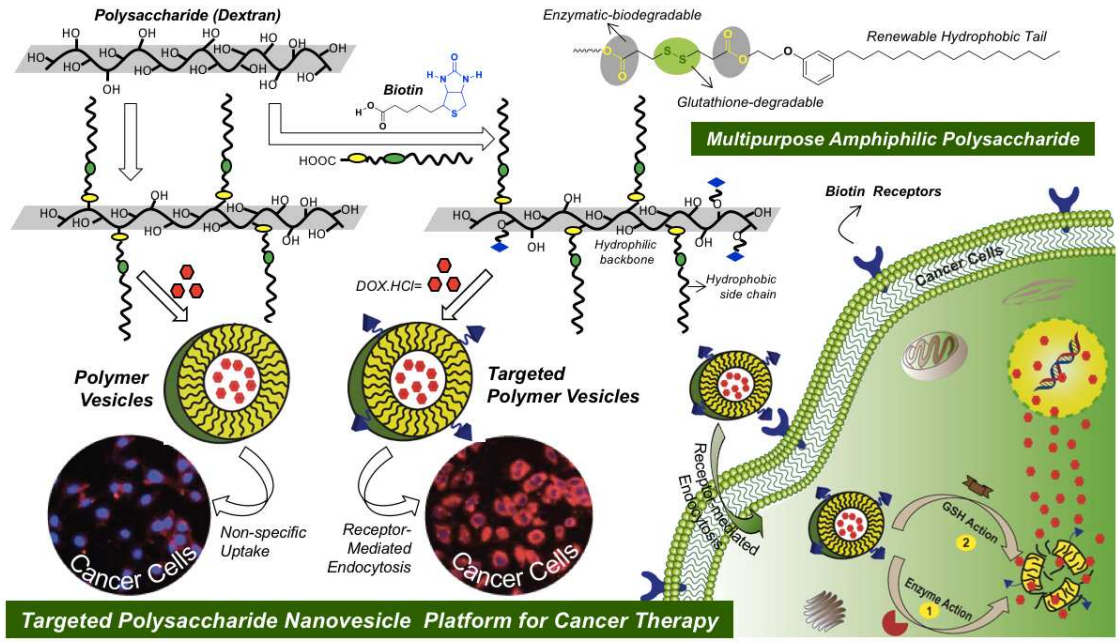

Figure 1. *Biotin-tagged polysaccharide nano-vesicular assemblies for receptor-mediated endocytosis in cancer cells and delivery of drugs at intracellular levels by GSH and enzyme multi-stimuli-responsiveness.*

The present investigation is emphasised to make new biotin-conjugated and multi-stimuli-responsive polysaccharide vesicles and demonstrate the proof-of-concept for water soluble anticancer drug DOX.HCl in cancer cells. The polymer vesicles were tailor made using redox and enzyme degradable chemical linkages containing renewable resource 3-pentadecylphenol hydrophobic unit. The present polysaccharide (dextran) vesicle has following features: (i) biotin-anchored at dextran backbone for receptor-mediated binding at cancer cell membranes, (ii) the PDP hydrophobic units was connected on the hydrophilic dextran backbone via disulphide (S-S) and aliphatic ester chemical linkages (see Figure 1), (iii) the high levels of glutathione (GSH) at the intracellular level (1 mM) compared to extracellular level (1 μM) act as redox-trigger[48] (*stimuli-1*) for the -S-S- bond cleavage (marked green in Figure-1) and disrupt the vesicular assembly for drug delivery, and (iv) the biodegradation of aliphatic ester linkages (marked yellow in Figure-1) by the esterase enzyme in lysosomal compartments[49-50] facilitated the drug release at the intracellular level (*stimuli-2*). The polymer vesicles provided unique opportunity to encapsulate water soluble anticancer drug doxorubicin-hydrochlroride (DOX.HCl) and deliver them to cancer cells using receptor-mediated endocytosis. The nanovesicles produced were < 180 ± 30 nm in size and Avidin-

HABA assay established the biotin-receptor affinity up to 25 nM concentration. *In vitro* studies revealed that the nanovesicles are stable under extracellular conditions and released drugs in response to intracellular stimuli such as GSH and esterase enzyme. The receptor-mediated endocytosis studies were performed in cervical cancer (HeLa) and WT-MEF (normal) cell lines. Time-dependent uptake studies by confocal microscope and FACS technique confirmed the occurrence of receptor-mediated endocytosis by biotin-tagged dextran vesicles. This was further corroborated by the time-dependent cytotoxicity studies wherein the cancer cells were found to be killed much better while delivering DOX.HCl from biotin-tagged vesicular platform compared to biotin free nano-vesicles. In a nut shell, the present investigation provides first insights into the administration of water soluble anticancer drugs through receptor-mediated endocytosis based on biotin-tagged dextran vesicles and it opens up new opportunities for the development of targeted polymer vesicular nano-carrier platform for long term application in cancer treatment.

Experimental Section

Materials and Methods: 3-Pentadecylphenol (PDP), 2-bromoethanol, triethylamine, dextran (Mol. wt 6000), N-(3-dimethylaminopropyl)-N-ethylcarbodiimide hydrochloride (EDC.HCl), 4-dimethylamino pyridine, dithiothreitol (DTT), glutathione (GSH), doxorubicin hydrochloride (DOX.HCl), dicyclohexylcarbodidimide (DCC), 4-dimethyl amino pyridine (DMAP), biotin and horse liver esterase enzyme were purchased from Aldrich chemicals. Avidin was purchased from Alfa aesar and used as such. 4'-hydroxyazobenzene-2-carboxylic acid (HABA) was purchased from Loba Chemie and used as received. NaOH and all other necessary reagents and solvents like dimethylsulfoxide (DMSO), N,N-dimethylformamide (DMF) and dichloromethane (DCM) were purchased locally and purified following the standard procedures. The instrumentation details, structural characterization, biological data collection for MTT assay, confocal imaging and Flow cytometry analysis, tissue culture conditions, and the synthesis of compound (**1**) are given in the supporting information.

Synthesis of 3-((3-oxo-3-(2-(3-pentadecylphenoxy) ethoxy) propyl) disulfanyl) propanoic acid (2): 3, 3'-Dithiopropionic acid (DTPA) (5.0 g 24 mmol) and compound (**1**) (4.14 g 12 mmol) were dissolved in 100 mL dry THF and purged with nitrogen for 10 minutes. To the

above mixture, DCC (3.19 g, 16 mmol) and DMAP (0.43g, 4 mmol) dissolved in dry THF was added and the reaction continued for 12h at room temperature. Dicyclohexyl urea from the reaction mixture was separated by filtration and the organic solvent was evaporated. The product was purified by passing through silica gel column 60-120 mesh using 5 % ethyl acetate: pet ether solvent system. Yield = 5.8 g (36.0 %) ^{1}H NMR (400 MHz, d_6-DMSO) δ = 12.36 (s, 1 H), 7.16 (t, *J* = 7.9 Hz, 1 H), 6.81 - 6.67 (m, 3 H), 4.36 (dd, *J* = 3.8, 5.5 Hz, 2 H), 4.21 - 4.08 (m, 2 H), 2.97 - 2.82 (m, 4 H), 2.78 - 2.71 (m, 2 H), 2.64 - 2.57 (m, 2 H), 1.60 - 1.48 (m, 2 H), 1.34 - 1.18 (m, 24 H), 0.89 - 0.80 (m, 3 H).. ^{13}C NMR (100 MHz, d_6-DMSO) δ: 172.4, 170.9, 158.0, 143.8, 128.9, 120.6, 114.3, 111.3, 65.2, 62.7, 39.9, 39.7, 39.5, 39.1, 38.9, 38.7, 35.0, 33.3, 33.1, 32.8, 32.4, 31.1, 30.6, 28.8, 28.8, 28.8, 28.7, 28.5, 28.5, 21.9, 13.7. MALDI TOF−TOF (MW: 540.27):m/z = 563.28 (M + Na) +. HR-MS (ESI+): m/z [M + H] + Calcd for $C_{29}H_{48}O_5S_2$ [M] +, 541.2978; found, 541.3019

Synthesis of DEX-SS-PDP: Dextran (M_w= 6,000, 1.0 g, 6.2 mmol of anhydroglucose unit), compound (**2**) (1.0 g, 1.83 mmol) were dissolved in anhydrous DMSO+DMF+DCM solvent mixture (15.0 mL: 8.0 mL: 2.0 mL). The formed reaction mixture was purged with dry nitrogen. To the above content, DMAP (0.22 g, 1.86 mmol) in DMSO (3.0 mL) and EDC.HCl (0.52 g, 2.72 mmol) in DMSO (3.0 mL) were added. The reaction mixture was stirred for 24 hour at room temperature. DMSO was removed; the liquid was precipitated in acetone. The purification was repeated at least twice to get pure dextran derivative which was dried under vacuum at 60 ^{o}C and stored. Yield = 0.65 g (65 %). ^{1}H NMR (400 MHz, d_6 DMSO) δ: 7.17-7.01 ppm (s, 1H, Ar-H), 6.76 - 6.72 ppm (m, 3H, Ar-H), 4.93, 4.85, 4.51 ppm (s) 4.68 ppm (s), 4.35ppm (t, 2H, Ar-O-CH_2), 4.16 ppm (t, 2H, -CH_2-OH), 3.14-3.69 ppm, 2.96 - 2.92 ppm (m, 4H, -CH_2-CH_2-S-S-), 2.76 - 2.72 (m,4H, -S-S-CH_2-CH_2-), 2.49 ppm (2H, Ar-CH_2), 1.53 ppm (2H, Ar-CH_2-CH_2), 1.18-0.80 ppm.

Synthesis of DEX-SS-PDP-Biotin: Dextran (M_w= 6,000, 1.0 g, 6.2 mmol of anhydroglucose unit), compound (**2**) acid (1.0 g, 1.83 mmol) and biotin (60.0 mg, 0.25 mmol) were dissolved in anhydrous DMSO+DMF+DCM solvent mixture (15.0 mL: 8.0 mL: 2.0 mL). The formed reaction mixture was purged with dry nitrogen. To the above content, DMAP (0.25 g, 2.04 mmol) in anhydrous DMSO (3.0 mL) and EDC.HCl (0.59 g, 3.08 mmol) in anhydrous DMSO (3.0 mL) were added. The rest of the procedure is followed as described for **DEX-SS-**

PDP. Yield =0.76 g(70 %). ^{1}H NMR (400 MHz, d_6 DMSO) δ: 7.17-7.01 ppm (s, 1H, Ar-H), 6.76 - 6.72 ppm (m, 3H, Ar-H), 6.42-6.36 ppm (biotin –NH protons), 4.93, 4.85, 4.51 ppm (s) 4.68 ppm (s), 4.35 ppm (t, 2H, Ar-O-CH_2), 4.27- 4.15 ppm (biotin –CH protons) 4.16 ppm (t, 2H, -CH_2-OH), 3.14-3.69 ppm, 2.96 - 2.92 ppm (m, 4H, -CH_2-CH_2-S-S-), 2.76 - 2.72 (m,4H, -S-S-CH_2-CH_2-), 2.49 ppm (2H, Ar-CH_2), 2.15 ppm (s, 2H, biotin –CH_2), 1.60-1.30 (broad, 6H, biotin –CH_2), 1.53 ppm (2H, Ar-CH_2-CH_2), 1.18-0.80 ppm.

Lysosomal Tracking of the Nanovesicles: In a typical experiment, 25000 cells were seeded in each well in live cell chamber and allowed to adhere for 16-18 h. Further these cells were treated with required concentration of Fluorophore and incubated for another 6h. Finally the media was aspirated and cells were washed two times with PBS (1X) and cells were treated with 1.0 mL of DMEM media having 25.0 nM of Lysotracker green DND-26 and cells were imaged immediately.

Cellular Uptake at 4 ºC: In a typical experiment, 50000 cells were seeded in each well of six well plate and allowed to adhere for 16h. Media from the cells was then aspirated and fresh media containing the Dox loaded nanovesicles was added and cells were incubated at 4 ºC (on Ice) for 0.5 h and finally fixed using paraformaldehyde. These cells were imaged using the confocal microscopy.

Cellular Uptake using Biotin Pre-treatment: 100000 cells were seeded in each well of six well plate and allowed to adhere for 16 h. After 16 h, cells were treated with fresh media having 2.0 mM biotin concentration and incubated for another 1h at 37 ºC. Finally the media containing biotin was aspirated and cells were treated with fresh media having required concentration of Dox loaded nanovesicles and incubated for another 4 h at 37 ºC. Finally cells were then fixed using paraformaldehyde and imaged using confocal microscopy.

Results and Discussion

Synthesis of Biotin-Conjugated Dextran

Biotin conjugated and dual responsive dextran derivatives were synthesized as shown in the scheme 1. A renewable resource and vesicular structure directing hydrophobic molecule 3-pentadecyl phenol (PDP)[41] from cashew nut shell liquid was coupled with 2-bromoethanol to yield the compound (**1**). The compound (**1**) was coupled at one end of the dithiopropionic acid through aliphatic ester linkages to yield compound (**2**). This hydrophobic unit (**2**) has the disulfide bond (-S-S) which is redox-degradable by glutothione (GSH) at intracellular compartmnets of cells (stimuli-1). The coupling of compound **2** in the dextran backbone produced DEX-SS-PDP. The conjugation of both compound **2** and biotin in the polysaccharide backbone in one-pot reaction yielded DEX-SS-PDP-Biotin. The reaction of biotin and dextran produced DEX-Biotin and its structure is shown in the supporting information scheme-**S1**. Both compound **2** and biotin were conjugated in the dextran backbone via aliphatic ester linkages that are enzymatically-biodegradable (stimuli-2) at the intracellular compartments. The structure of dextran derivatives were confirmed by ^{1}H-NMR. In figure 2a, the PDP substituted unsymmetrical dithiopropionic acid molecule (**2**) showed expected number of protons and they are alphabetically assigned in the chemical structure. The carboxylic ester -$SCH_2C\mathbf{H}_2COOR$ (proton i) and carboxylic acid $SCH_2C\mathbf{H}_2COOH$ (proton L) appeared at 2.73 and 2.59 ppm, respectively. In figure 2b, up on anchoring onto the dextran backbone, the carboxylic acid (proton L) vanished and the new ester peaks appeared together (proton i+L, double the intensity). Additionally, the DEX-SS-PDP-Biotin dextran derivative showed peaks corresponding to PDP units at 6.8 to 7.3 ppm. The broad peak at 6.5 ppm was assigned to N-H protons in biotin unit (proton m) and the new ester peak with respect to biotin conjugation in the dextran backbone appeared at 2.43 ppm (proton n). These peak assignments were further confirmed by comparing the ^{1}H-NMR spectra of DEX-SS-PDP (see S2) and DEX-Biotin (see S3) in supporting information. The degree of substitution of disulfide PDP on dextran backbone was determined by comparing the peak intensities of PDP aromatic protons at 6.8 ppm (proton e+f) or aliphatic protons of PDP (protons j+k) with dextran anomeric proton 4.6 ppm (proton p). The degree of substitution for biotin conjugation was determined by comparing the peak intensity of the biotin N-H peak at 6.4 ppm (proton-m) or ester peak at 2.43 ppm (proton n) with anomeric proton at 4.6 ppm (proton p). The degree of substitution of PDP and biotin were estimated to

be 5.0 % and 2.0 %, respectively. The higher incorporation of PDP + biotin (more than 10 % in total) in the dextran backbone produced water insoluble polymers; thus the total degree of substitution was restricted to less than 10 %. TGA and DSC analysis of the polymer derivatives showed their thermal stability up to 250 °C and they were found to be largely amorphous polymers (see S4).

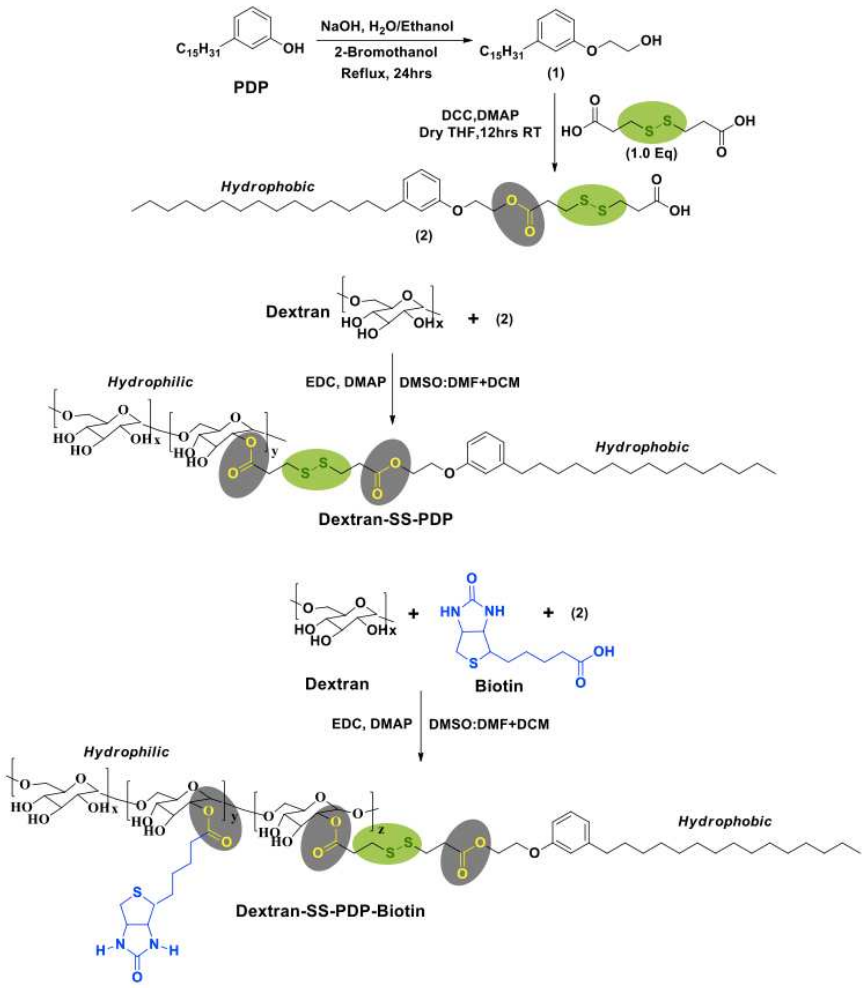

***Scheme1**: Synthesis of enzyme and GSH dual responsive and biotin-conjugated dextran derivatives.*

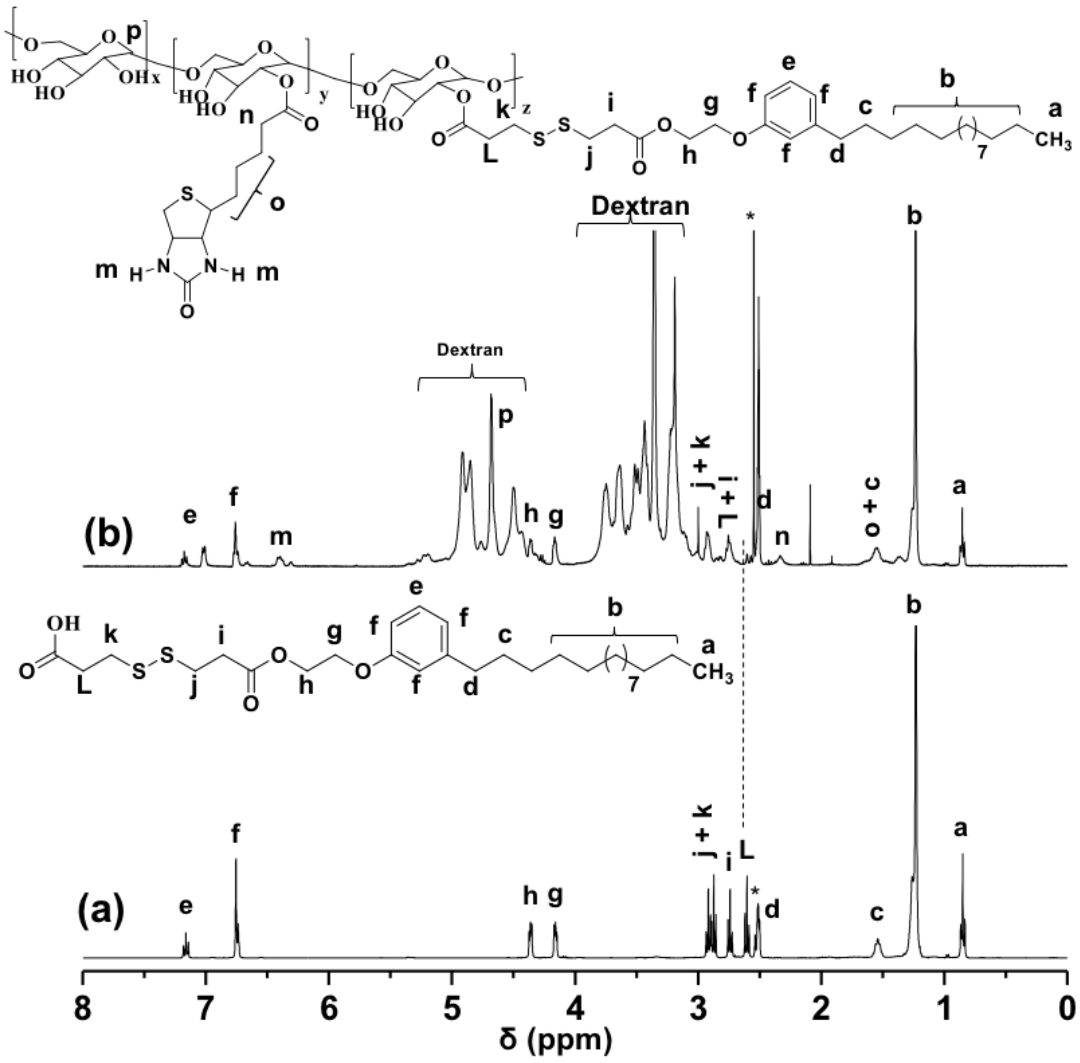

Figure 2: *^{1}H-NMR spectra of compound 2 (a) and DEX-SS-PDP-Biotin (b) in d_6-DMSO. The solvent peaks are assigned by asterisk.*

Dextran Nano-vesicles and DOX.HCl Encapsulation

In the present investigation, the hydrophilic polysaccharide backbone (dextran) was conjugated with hydrophobic amphiphilic unit based on PDP; thus in aqueous medium, the hydrophobic chain oriented away from the water to give amphiphilic sheet-like geometry. The inter-digitations of PDP chain from the apmphiphilic dextran resulted in bi-layer self-assemblies which folded into vesicular architectures through cooperative interactions. The evidence for the PDP chains inter-digitations in the vesicular geometry was proved by single crystal structure analysis of PDP units in our earlier work.[51-52] Thus, it is anticipated that the

PDP + dithiopropionic ester linkages in the present design is also expected to follow similar inter-digitation to produce well-defined dextran vesicles (see Figure 3a). To study the self-assembly behaviours of newly designed dextran derivatives DEX-SS-PDP-Biotin, DEX-SS-PDP, and DEX-Biotin; they were subjected to dialysis in water. Typically, dextran derivatives were dispersed in water + DMSO and dialysed using semi-permeable membrane of MWCO=3500 in milli-Q water. The dialysate was replenished with fresh water periodically to remove DMSO and at the end of 48 h of dialysis, a transparent solution was produced (see Figure 3) which was lyophilized and stored at 4 °C. These dialysed dextran derivatives were subjected to dynamic light scattering (DLS) and atomic force microscope (AFM) analysis.

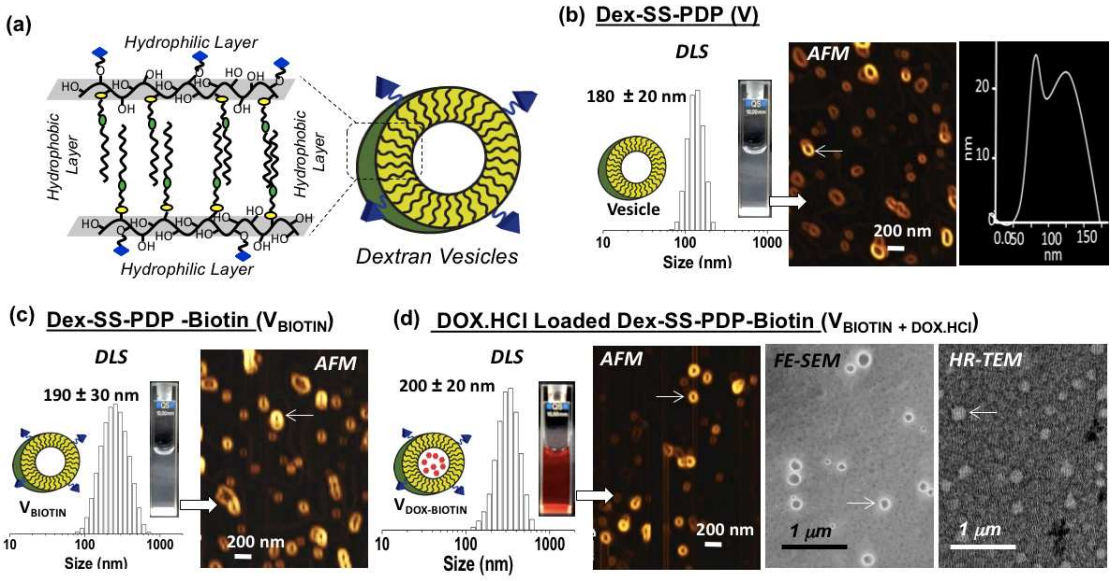

Figure 3*: (a) Self-assembly of dextran derivative into vesicles. (b) DLS histogram and AFM images of DEX-SS-PDP vesicles (V). (c) DLS histogram and AFM images of DEX-SS-PDP-Biotin vesicles (V_{BIOTIN}). (d) DLS histogram, AFM, FESEM and HRTEM images of DOX.HCl encapsulated DEX-SS-PDP-Biotin vesicles ($V_{BIOTIN+DOX.HCl}$).*

In figure 3b, DLS histograms of DEX-SS-PDP showed monomodal distribution with size 180 ± 20 nm. AFM is a very powerful tool to study the morphological features of soft-materials such as vesicles created from aqueous medium.[41] AFM images of DEX-SS-PDP in figure 3b appeared as donut-shaped spherical objects with diameter 180 ± 30 nm with height of the nano vesicles around 20 ± 10 nm (see Figure 3b). The sizes of the nano-vesicles in

AFM image exactly matched with the DLS nano-aggregates in aqueous medium confirming that vesicular self-assembly was indeed created and preserved in the aqueous medium through the hydrophilic and hydrophobic interaction as represented in figure 3a. DLS histograms and AFM images for DEX-SS-PDP-Biotin are shown in figure 3c. The size of the assembly from DLS and AFM images were obtained as 190 ± 30 nm and 200 ± 20 nm, respectively, indicating that the vesicular nano-assembly was perfectly preserved in the biotin conjugated dextran derivative as well. DLS and AFM data for DEX-biotin (without SS-PDP unit) revealed that the polymer structure produced nanoparticles rather than vesicles. This emphasised the need of SS-PDP unit in the dextran backbone to produce vesicular geometry (see S5) and the result was in accordance with our earlier observation[41,47] that the PDP unit was essential to self-assemble the dextran backbone into nano-vesicles in aqueous medium. Further static light scattering (SLS) studies were carried out to establish the nano-vesicle aggregates in solution state (see S6). SLS gives the radius of gyration (R_g) of the polymer assemblies and DLS provides the hydrodynamic radius (R_h) of the polymer nano-assemblies. The ratio of the R_g/R_h =1 for polymer nano-vesicles as reported in the literature.[53-54,41] In the present investigation, the R_g = 70 nm was obtained as from SLS and R_h = 73 nm from DLS; thus the ratio R_g/R_h = 70 nm / 73 nm = 0.96 ≈ 1.0, which confirmed the formation of polymer nanovesicles in the solution state. The size of the nano-vesicles is matched very well with the DLS, AFM, FESEM and HRTEM images as shown in figure 3. To study the role of concentration of polymer on the nanovesicle formation, the self-assembly was carried out by dialysis method by varying the concentration from 0.001 to 1.0 mg/mL (1000 time dilution). DLS data of these dialyzed solutions (see S7) revealed that the size of the nanovesicles were almost retained in the same range of 220 ± 20 nm irrespective of the variation in the concentration of polymer solution. Thus, we believe that the polymer vesicles formation was largely driven by the structure rather than concentration. Hence, the present design could produce vesicles of 200 ± 20 nm in size which is in the acceptable range for EPR effect.[55]The above dextran nano-vesicles DEX-SS-PDP and its biotin conjugated analogue DEX-SS-PDP-Biotin are hereafter referred as V and V_{BIOTIN}, respectively. The critical vesicular concentration of the dextran vesicles was determined using pyrene as probe.[41] A fixed amount of pyrene (0.6μM) was used and the concentrations of the dextran conjugates were varied from 2.4×10^{-7} to 4.8×10^{-5} M. From the ratio of the pyrene characteristic peaks (I_1/I_3), the critical vesicular concentration was determined as 2.4×10^{-6}

M (see S8). One of the unique features of vesicles or polymersomes is that they possess hydrophilic core for encapsulation of water soluble fluorophore dye like Rhodamine B (RhB) and water soluble anticancer drugs such as doxorubicin-hydrochloride DOX.HCl which are not possible in micelles or nanoparticles.[44] To study the encapsulation capability of newly designed dextran vesicles, V and V_{BIOTIN} were subjected for encapsulation of RhB and DOX.HCl by dialysis method using semi-permeable membrane MWCO = 3500 Da as described earlier. The DLS histogram of $V_{BIOTIN+DOX.HCl}$ showed the size of the nano-vesicles as 200 ± 20nm (see Figure 3d). AFM morphology confirmed the donut-shaped features with respect to vesicular morphology. Field mission scanning electron microscope (FESEM) and transmission electron microscope (TEM) images further confirmed the spherical nature of the vesicular nano-assemblies with difference in contrast with respect to the layer and core (see Figure 3d). DLS, AFM, FESEM and HR-TEM images showed the sizes < 200 nm and confirmed existence of the dextran nano-vesicles. $V_{DOX.HCl}$ (without biotin conjugation) and V_{RhB} and $V_{BIOTIN+RhB}$ were also found to exist as nano-vesicles (see S9). Using absorption spectroscopy, the drug (or dye) loading content (DLC) was obtained in the range of 1.5 to 2.0 %. The drug (or dye) loading efficiency (DLE) was typically obtained in the ranges of 50 to 60 % (see S-9). The absorbance and fluorescence spectra for RhB and DOX.HCl encapsulated nano-vesicles showed very good red-emission suitable for bio imaging process (see S10). Other method like sonication was also explored for the encapsulation of DOX.HCl in the vesicles. The sonication method gave much higher DLC = 37 %. However, further dialysis of the sonication-assisted sample exhibited premature leaching of the drug. At the end of the dialysis , the DLC was obtained as 1.8 % which is similar to that of direct dialysis process (without prior sonication). Hence, the dialysis procedure is the one of the best way to encapsulate water soluble drugs to produce stable Dox formulation in polysaccharide vesicles.

Avidin-Binding Assay and Stimuli-responsive Delivery

The dextran vesicles are designed with three components which are responsive to cancer cells both at the extracellular and intracellular environments. These responsiveness are: (i) receptor-assisted endocytosis process at the periphery of the cell membranes (see Figure 4a), (ii) redox-cleavable disulfide (S-S) chemical linkages to disassemble the vesicular assemblies by glutathione (GSH) residue in the cytosol, and (iii) lysosomal enzymatic-

biodegradation of aliphatic ester linkage connecting the hydrophobic unit at the dextran backbone (see Figure 4b). To study the receptor-mediated biological events, *in vitro* experiments were designed based on Avidin-HABA assay [19,56-57] and the data is summarized in Figures 4c and 4d. Avidin has four binding sites for HABA (4'-hydroxyazobenzene-2-carboxylic acid); thus, 1:4 complex of Avidin-HABA was produced following the reported procedure.[19] Avidin-HABA complex showed unique absorption peak at 505 nm which is completely distinguished from either HABA or avidin (see S11). This avidin-HABA complex was titrated with biotin conjugated vesicles (V_{BIOTIN}) and normal vesicles (V) and the data are shown in figure 4c. As shown in figure 4c, there is a gradual decrease in the absorption of Avidin-HABA complex at 505 nm with the increase in the concentration of V_{BIOTIN}. Interestingly, the non-biotin conjugated vesicles (V) did not show any changes in the absorption maxima of Avidin-HABA complex (see red line in Figure 4c). This further confirmed that the biotin free vesicles (V) do not possess any binding towards Avidin. This trend clearly indicates that the HABA molecules are getting replaced by the V_{BIOTIN} in the Avidin-HABA complex. The reason for this replacement of HABA molecules by V_{BIOTIN} samples can be attributed to the higher association constant for Avidin-Biotin compared to that of Avidin-HABA complex.[8] Thus, the decrease in the absorbance maxima followed by the additions of V_{BIOTIN} is arisen followed by the complexation of Avidin-biotin at the periphery of biotin conjugated (V_{BIOTIN}) nanovesicles. This decrease in the absorption was plotted as $[(A_0-A_C)/A_0]$ versus concentration of the biotin in the vesicles, where A_0 is the initial absorbance and A_C is the absorbance at concentration 'C'. As can be seen from the figure 4d, the value of $[(A_0-A_C)/A_0]$ steadily increases and saturated at 25 nM. From the break point in the plot, it can be assured that the avidin-biotin interactions saturated at 25 nM of biotin at the periphery of vesicles. The number of biotin molecules per polymer chains were determined by the method reported by Karen Wooley and co-workers.[19] It was found to be approximately one molecule of biotin present in each polymer chain (see S12 for more details) .The affinity of the biotin-nanovesicles towards Avidin is in accordance to the other polymer systems.[19,56-57] Thus, the current dextran vesicle possess significant amount of biotin to bind streptavidin like membrane protein on cancer cells surface for targeted delivery. To differentiate the circulating free biotin and biotin-conjugated vesicles towards their molecular interaction with avidin like receptors under physiological conditions, competitive binding assay was studied in fetal bovine serum (FBS) (see Figure S13). Interestingly, there was no

replacement of HABA molecules from avidin-HABA complex by the residual biotin present if at all in FBS. The addition of biotin conjugated vesicles (V_{BIOTIN}) into this avidin-HABA complex in FBS immediately showed decrease in the spectroscopic signal at 505 nm with respect to the binding of biotin-conjugated vesicles (V_{BIOTIN} vesicles) in the avidin pocket. This control experiment provides direct evidence for the targeting ability of biotin-conjugated vesicles towards the membrane receptors under physiological conditions.

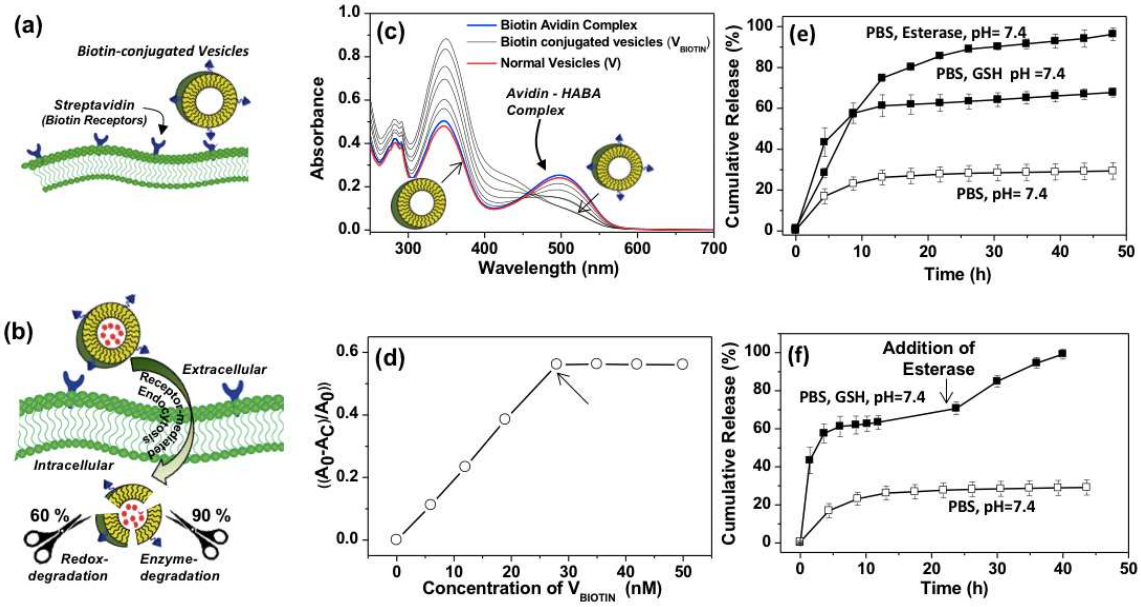

Figure 4. *(a) Receptor mediated binding of biotin conjugated vesicles (V_{BIOTIN}) on the cell membrane. (b) GSH-assisted redox-degradation and enzymatic-biodegradation of nanovesicles at the intracellular compartments. (c) Absorbance spectra of the Avidin-HABA complex upon additions of biotin conjugated dextran vesicles (V_{BIOTIN}) and biotin free vesicles (V). (d) Plot of* $[(A_0-A_C)/A_0]$ versus *the concentration of V_{BIOTIN}. (e) Cumulative drug release plots showing the release of DOX. HCl from $V_{BIOTIN+DOX.HCl}$ vesicle in PBS at pH 7.4, 37°C, incubated in presence of 10 mM GSH, and incubated in presence of 10 U esterase enzyme. (f) Drug release plot showing the DOX release from $V_{BIOTIN+DOX.HCl}$ in PBS at pH 7.4 in presence of 10 mM GSH for 24 h and subsequent addition of 10 U of esterase enzyme.*

The dextran vesicles are designed with two intracellular stimuli to break nano-carriers to release the drugs. Glutathione (GSH) is largely present in the cytosol of the cells and its concentrations vary significantly from extracellular (1.0 *μM)* to intracellular level (1.0 mM)[48]. The polymer nano-carriers built with disulphide chemical linkages are susceptible to undergo redox-degradation by GSH[48] (see Figure 4b). In the present case, the vesicles were constructed with –S-S- linkages in the hydrophobic units; thus, *in vitro* drug release kinetic

studies were carried out for the DOX.HCl loaded nano-vesicles by exposing them to GSH in PBS. The GSH cleavage of the hydrophobic tail ruptured the nano-vesicular structure and the DOX.HCl gets released. The cumulative drug release was estimated by measuring the absorbance of DOX.HCl in the reservoirs and the release profile is shown in Figure 4e. In the absence of GSH, about 20 % drug leaching was observed due to the presence of salts in PBS. The anions like PO_4^{2-} in PBS are well-known to influence on the stability of the polymer nano-assemblies through Hofmeister effect and salting-out of macromolecules in solution.[58] The PO_4^{2-} anion is typical salting-out type which induces the partial phase separation of the polymer nano-assemblies in PBS which accounts for 20% leaching.[59] The stability of the dextran vesicles was further checked in FBS and since FBS are free of ions , DLS studies showed that the vesicles are stable for more than 24h (see S14). The release was significantly influenced by the presence of GSH and about 60 % drug was released in a controlled manner. This suggested that once the nano-vesicles enter the cytosol, the GSH could partially disassemble the vesicles to release about 60 % of the drugs. Another important process in which the nano-vesicles are transported and digested across the cell membrane is mediated by endosome-lysosome compartments. Lysosomes typically have large abundance of digestive enzymes such as α-chymotrypsin, trypsin, esterase and phosphatase, etc[60]. Among this esterase enzyme could readily biodegrade aliphatic ester chemical linkages[49] to deliver the drugs. Aliphatic ester-linkages are readily susceptible to undergo lysosomal enzymatic biodegradation and this concept has been proven very well by us and few others in L-amino acids based polyesters,[49] poly(ester-amide)s,[60] substituted polycaprolctone block copolymers[61] and PEG-PLLA copolymers.[62] In the present design, the hydrophobic tail was conjugated with dextran using aliphatic ester chemical linkages (see Scheme-1). Thus, the *in vitro* drug release profile data shown in Figure 4e in the presence of esterase enzyme in PBS is direct proof for the enzymatic biodegradation of the polysaccharide vesicles. Esterase enzyme docking studies from our lab[45] had shown that the dextran-PDP ester linkage readily occupied the enzymatic pocket for biodegradation. Since the present vesicular structure has been built with aliphatic ester linkages that connect the hydrophobic unit in the dextran backbone, esterase enzyme was employed as stimuli to study the drug release kinetics. In figure 4e, the drug release pattern was found much higher for esterase enzyme exposure and almost 90 % DOX.HCl was released in 12 h. In order to study the combination effect of GSH and esterase-enzyme action together, the nano-vesicles were initially subjected to GSH

incubation for 24 h and subsequently esterase enzyme was added. In this process, the release kinetics data in figure 4f showed GSH could release 60 % drugs and the remaining 40 % drug was essentially released by esterase. Hence, the combination of GSH and esterase enzyme stimuli are very good triggers to release water soluble DOX.HCl in controlled manner at the intracellular compartments of cells. Similarly, the non-biotin conjugated dextran vesicles were also subjected to drug release studies for GSH and enzyme responsiveness (see S-14). The drug release patterns were found almost identical in both biotin-conjugated (see Figure 4e) and biotin free dextran vesicles (see S15). To address the possibility of disassembly of nano-carriers in the cytosol by GSH and their further migration toward the endo-lysosomal compartment for biodegradation by enzymes; the drug release study was carried out by (i) initially incubating the DOX loaded polymer vesicles in the presence of esterase enzyme and then (ii) administrate glutathione (GSH, 10mM) in PBS. The drug release was done by dialysis method and monitored by absorption spectroscopy (S16). From the results, it is clear that the esterase enzyme predominantly released the drug (65-70 %) and the remaining 30 % of the drugs released by GSH. This experiment along with the data in Figure 4f suggests that enzyme and GSH responsiveness work together in the intracellular compartment to maximize the digestion of nanovesicles for drug release rather than in sequential manner. The above studies confirmed that the newly designed dextran vesicles are efficient triple action nano-carriers to undergo receptor mediated interaction at the cell membrane, readily cleavable by GSH in the cytosol, and also completely digested by esterase enzyme at the lysosomal compartments.

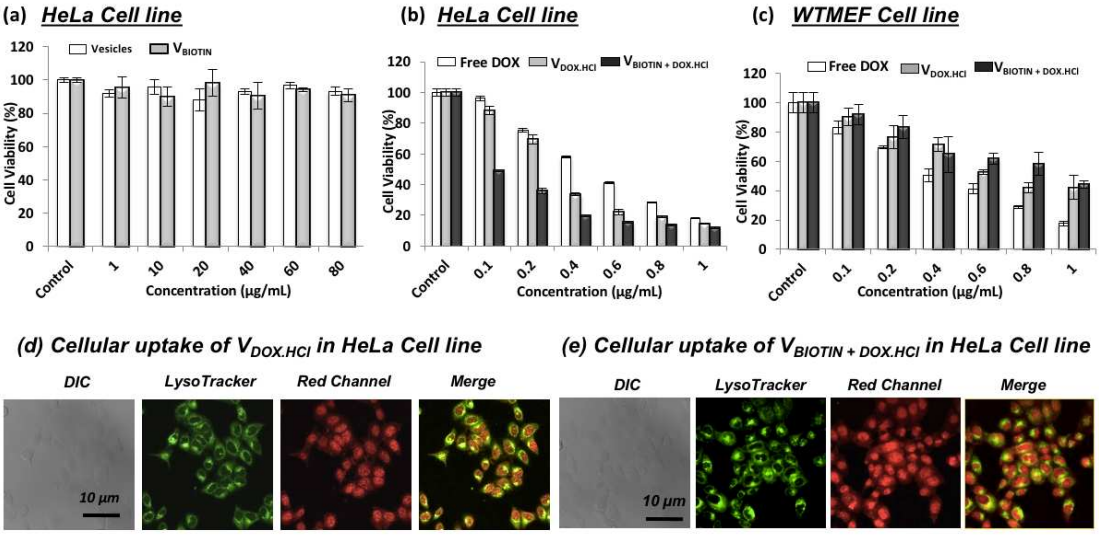

Figure 5. *(a) Histogram showing the cytotoxicity profiles of dextran vesicles (V) and* V_{BIOTIN} *in HeLa cell line. (b) Histogram showing the cytotoxicity profile for free DOX.HCl,* $V_{DOX.HCl}$ *and* $V_{BIOTIN+DOX.HCl}$ *in HeLa cell line. (c) Histogram showing the cytotoxicity profile for free DOX.HCl,* $V_{DOX.HCl}$ *and* $V_{BIOTIN+DOX.HCl}$ *in WT-MEF cell line. Live cell confocal microscopic images in HeLa cells for the uptake of* $V_{DOX.HCl}$ *(d) and* $V_{BIOTIN+DOX.HCl}$ *(e). The concentration of the Lyso tracker green and drug used are 25nM and 2 µM respectively. The cells were incubated for 4 h at 37º C.*

Cytotoxicity of the dextran vesicles was studied by MTT Assay. In cervical cancer cells (HeLa) and wild type mouse embryonic fibrolast (WT-MEF) cells (normal cell line), the dextran vesicles were found to be non-toxic to cells up to 80 µg/mL (see figure 5a and S17). DOX.HCl loaded dextran vesicles $V_{DOX.HCl}$ and $V_{BIOTIN+DOX.HCl}$ were treated in HeLa cells by varying the drug concentration ranging from 0.1 to 1.0 µg/mL. The vesicle assisted drug administration seems to be better in accomplishing cytotoxicity in HeLa cells compared to free drug (see Figure 5b). Cytotoxicity experiment was carried out in breast cancer cell line (MCF 7) and the data is shown in S-17a. The effect of cell killing by the DOX loaded nanovesicle in MCF 7 is almost identical to that of HeLa (cervical) cancer cell line (see Figure 5b). This suggested that the approach is not restricted to one particular cancer cell lines. Further among the vesicles, the biotin-conjugated vesicles $V_{BIOTIN+DOX.HCl}$ were able to achieve much better IC_{50} at a concentration of 0.1 µg/mL which is almost 5 times better than the IC_{50} of 0.5 µg/mL by free drugs. When DOX.HCl loaded dextran vesicles were tested in

WT-MEF cell line (normal cells, see Figure 5c), they showed relatively less cytotoxicity compared to free drugs. This observation is particularly important since the free drug is more toxic to the WT-MEF cells compared to cancer cells. DOX-loaded vesicles largely kill the cancer cells (> 90 %); however, the effect was much lower in the normal cells (< 50 %). To compare the cytotoxicity effect induced by the GSH stimuli, two types of polymer vesicles were employed for MTT assay. For this purpose (i) vesicles without disulfide chemical linkages in the hydrophobic part reported in our earlier work[46] and (ii) vesicles with disulfide linkages (V_{BIOTIN}, reported here) were employed. It is important to mention that both types of vesicles have aliphatic ester linkages that connect the hydrophobic part in the dextran backbone; thus, these vesicles are readily biodegradable by lysosomal enzymes. These nanovesicles were encapsulated with DOX and their cytotoxicity data was carried out in breast cancer cells (MCF 7) and the details are summarized in S18a and S18b. It is very clear from the data that the disulfide containing vesicles exhibited comparatively better killing at higher concentration compared to the non disulfide vesicles. The data validated that GSH accelerated rupturing of the disulfide containing nanovesicles at the intracellular compartments. To study the cellular internalization and localization of the DOX.HCl loaded dextran vesicles and the digestion of dextran vesicles in the lysosomal compartments, live cell imaging was done using lyso-tracker in confocal scanning electron microscopy (see Figures 5d and 5e). The dextran vesicles $V_{DOX.HCl}$ and $V_{BIOTIN+DOX.HCl}$ showed significant amount of drugs at the nucleus and cytoplasm in red channels with respect to DOX emission. The lysosomes are stained in green colour and upon merging with the red channel, the merged images showed yellow colour in the cytosol and red in the nucleus. The yellow emission from the cytosol is an outcome of the co-localization of red emitting DOX and green lyso-tracker. This study confirmed that the dextran vesicles are indeed digested in the lysosomal compartments in cytosol. The DOX.HCl released from the vesicles accumulated in the nucleus to exhibit strong red-emission. From the above *in vitro* results, it can be concluded that the custom designed dextran vesicles can be used for targeting the biotin receptor that are overexpressed in cancer cells as well as high cytotoxicity can also be achieved through GSH and lysosomal-enzyme stimuli.

Receptor-Mediated Endocytosis

The uptake of nano-carriers in cells is typically controlled by four independent pathways: (i) Macropincytosis[63], (ii) direct endocytosis through hydrophobic like-like interactions between nano-carriers and membrane, (iii) endocytosis assisted by caveolae or clathrin proteins[64], and (iv) receptor-ligand interaction mediated endocytosis.[1-4] Among all these processes, the receptor-ligand mediated process seems to be very effective since many cancer cells are over expressed with multiple receptors for folic acid, biotin and RGD peptide, etc. To study the role of the receptor-mediated endocytosis process, two cell lines are chosen that are reported to have large difference in their membranes for biotin-receptors. Cervical cancer cells (HeLa) were found to be significantly over expressed with biotin-receptors compared to WT-MEF cells (normal cells).[17] Biotin receptor over expression is one of the well proven concept in HeLa cell line (cervical cancer) and HeLa cells were widely used by previous researchers to study the receptor-mediated uptake in biotin-tagged nano-assemblies and biotin-tagged polymer nanoparticles.[9,16-21,55,56] Hence, the HeLa cell line was chosen in the present investigation for studying the biotin receptor-mediated endocytosis in the newly designed biotin-tagged polysaccharide vesicles. The cellular uptake and intracellular localisation of the dextran vesicles $V_{DOX.HCl}$ and $V_{BIOTIN+DOX.HCl}$ was monitored by the confocal (CLSM) microscopy. Biotin conjugated and non-conjugated dextran vesicles were treated in these two different cell lines by varying the incubation time from 30 minutes to 360 minutes (6 h). The images in the figure 6a showed the cellular uptake of $V_{BIOTIN+DOX.HCl}$ vesicles with increasing incubation time. It is very clear from the images that the red fluorescence intensity from DOX.HCl gradually increased with the incubation time indicating that more drugs are taken up by the cells over a period of time. The fluorescence intensity from the images almost saturated at 6 h. The images for non-biotin conjugated vesicles $V_{DOX.HCl}$ showed increment in the fluorescence intensity with incubation time (see Figure 6b); however, the intensities of DOX emission were relatively low compared to the biotin conjugated vesicles. Free DOX.HCl was used as control and the cellular uptake images were recorded for 30, 120 and 360 minutes incubation. The free DOX uptake was relatively poor when compared to their delivery from biotin-conjugated vesicles (S19).

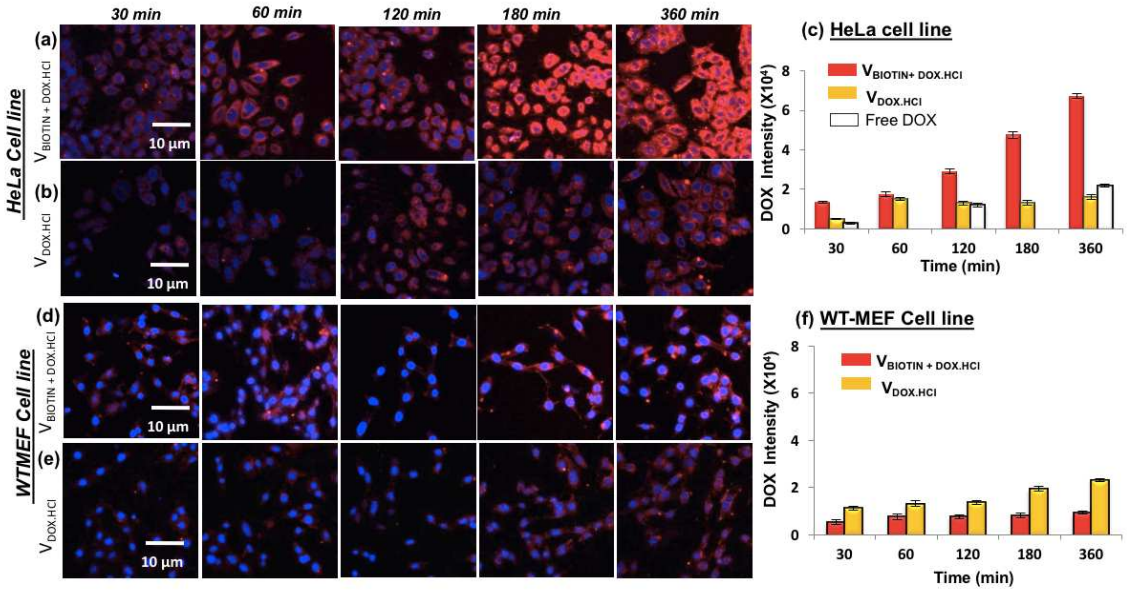

Figure 6: *Confocal microscopic images of (a) $V_{BIOTIN+DOX.HCl}$ and (b) $V_{DOX.HCl}$ in HeLa Cells at various incubation time. (c) The plot showing the corrected total cell fluorescence of DOX estimated from the confocal images in the right side panels (a and b) for various incubation time in HeLa cell line. Confocal microscopic images of (d) $V_{BIOTIN+DOX.HCl}$ and (e) $V_{DOX.HCl}$ in WTMEF cells at different time intervals. (f) The plot showing the corrected total cell fluorescence of DOX estimated from the confocal images in the right side panels (d and e) for various incubation time in WTMEF cell line. The concentration of the DOX.HCl was maintained as 2 µg/mL and the various incubation times are shown in the panel.*

The DOX intensity in each panel in figure 6a (for biotin-conjugate vesicles), figure 6b (biotin free vesicles) and free DOX (S-18) in HeLa cell lines was determined by image J software and plotted and shown in Figure 6c for quantification and comparison. A similar approach was carried for each panel in Figure 6d (for biotin-conjugate vesicles) and figure 6e (biotin free vesicles) in WT-MEF cell lines as shown in Figure 6f. The plots in Figure 6c and 6f provide direct information on the uptake of the above vesicles in these two different cell lines which are significantly different in the amount of membrane receptor concentration [8,9,16] In figure 6c, it can be seen that there is 3 fold more uptake of DOX in case of $V_{BIOTIN+DOX.HCl}$ vesicles as compared to the $V_{DOX.HCl}$ vesicles in HeLa cell lines. The results revealed that in case of $V_{BIOTIN+DOX.HCl}$, the cellular internalization of drugs was significantly higher than $V_{DOX.HCl}$ proving that the biotin conjugation in the dextran vesicles indeed enhanced the DOX concentration at tumour cells. The healthy cells (WT-MEF cell line in Figure 6b) do not over express the biotin receptors; thus, the cellular uptake by the biotin-functionalized vesicles and

biotin-free vesicles do not show much difference in their cellular uptake. This is further evident from the comparison of the uptake by the biotin-functionalized vesicles in Figures 6a (in HeLa) and 6b (in WT-MEF) that the former one showed significant uptake compared to the latter. A similar experiment was carried out for $V_{BIOTIN+DOX.HCl}$ and $V_{DOX.HCl}$ in normal cell line (WT-MEF) and the images are showed in figures 6d and 6e. Both $V_{BIOTIN+DOXHCl}$ and $V_{DOX.HCl}$ did not so much increment in the cellular uptake with increasing the incubation period. This data was further supported by the plot of DOX intensity versus incubation time in Figure 6f. The comparison of HeLa and WT-MEF cell lines data revealed that the cancer cells have preferential uptake for Biotin conjugated dextran vesicles (V_{BIOTIN}) compared to biotin free vesicles (V). This observation is further supported by the enhanced cell killing by the dextran vesicles in HeLa when compared to WT-MEF cells (see Figures 5b and 5c). The lyso-tracker experiments indicated that the dextran vesicles were readily digested by both cell lines at the intracellular level; thus, the difference in the cellular uptake (see Figures 6) and cytotoxicity effect (see Figure 5) among HeLa and WT-MEF cells is attributed to the difference in receptor-mediated uptake. The enhanced uptake of $V_{BIOTIN+DOX.HCl}$ in HeLa cells is attributed to the enhanced receptor-mediated endocytosis process. It is important to mention that the esterase enzyme concentrations could be similar in both WT-MEF and cancer cells for biodegradation; however, the higher receptor-mediated uptake in cancer cells allowed more uptake of biotin-targeted nanovesicles (see Figure 5). Thus, the selectivity accomplished in cancer cell is assisted by receptor mediated endocytosis process for increasing the drug payload in cancer cells (see Figure 6). The higher accumulation of drug carrier in cancer cells enabled enhanced cell killing in cancer cells compared to WT-MEF cells. Thus, the selectivity is accomplished in the present design by merging both intracellular biodegradation along with receptor-mediated endocytosis. To validate the receptor-assisted cellular uptake observation in confocal image, time-dependent flow cytometry analysis (uses live cell counting) was carried out for free DOX, V_{DOX}, and $V_{BIOTIN+DOX.HCl}$ in HeLa cell line. In figure 7a, the $V_{BIOTIN+DOX.HCl}$ and $V_{DOX.HCl}$ were found to exhibit almost 1.5 and 2.0 times, respectively, higher uptake than free DOX. The incubation time dependent flow cytometry data in Figure 7b further indicates that the DOX was taken up by the cells in higher quantity with increase in the incubation time. The plot of DOX intensity versus incubation time (see Figure 7c) further validates this observation. The comparison of data at 9 h incubation for biotin-conjugated dextran vesicles and biotin free dextran vesicles further established the

enhanced uptake of $V_{BIOTIN+DOX.HCl}$ in HeLa cell line. The above results directly evidence that the biotin-conjugated dextran vesicles are excellent nano-carriers for anticancer drugs like DOX.HCl to selectively target cancer cells compared to WT-MEF cells. *In vivo* data is further required to support the receptor-mediated approach for long-term application in cancer therapy. Nevertheless, the present manuscript has demonstrated the receptor-mediated endocytosis process in polymer vesicle and the proof-of-concept is successfully demonstrated in cancer cell lines.

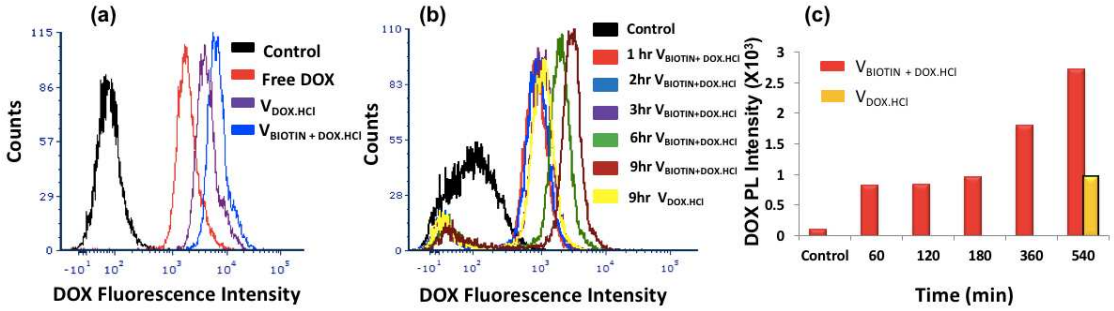

***Figure 7**: (a) Histogram showing the cellular uptake by flow cytometry analysis for free DOX.HCl, $V_{DOX.HCl}$ and $V_{BIOTIN+DOX.HCl}$ at 9h incubation. (b) Flow cytometry plots for $V_{DOX.HCl}$ and $V_{BIOTIN+DOX.HCl}$ at various incubation time. (c) The plot of DOX intensity against incubation time estimated from figures a and b and shown in bar diagram. The concentration of the DOX.HCl was maintained as 2 µg/mL and 10000 cells were counted for each experiment.*

Evidence for Receptor-mediated Endocytosis

Three control experiments were carried out to support the receptor-mediated cellular uptake in HeLa cell lines and they are: (i) cellular uptake studies of dextran vesicles in biotin pre-treated cancer cells, (ii) cellular uptake of dextran vesicles at low temperature by supressing the regular endocytosis process, and (iii) time-dependent cytotoxicty assay. To study the biotin-receptor mediated endocytosis of dextran vesicles; cellular uptake experiment was carried out in HeLa cells at 37 ºC using biotin pre-treatment. HeLa cells were pre-treated with 2 mM biotin for 1 h[65-66]. The pre-treated cells and control cells (without biotin pre-treatment) were subjected to $V_{DOX.HCl}$ and $V_{BIOTIN+DOX.HCL}$ and incubated for 4 h at 37 °C. Confocal microscope images in figure 8a showed the uptake of DOX from $V_{BIOTIN+DOX.HCl}$ in biotin-pre-treated HeLa cells. The biotin pre-treatment in the HeLa cells

were carried out to block all the receptors with free biotin; hence one would anticipate that the biotin-functionalized vesicles uptake in cells will be reduced due to the non-availability of the receptors on the cell membranes. The comparison of the uptake of the biotin-functionalized vesicles in HeLa cells indeed showed lower uptake in the biotin pre-treated cells due to the non-availability of receptors (see Figure 8a). This control experiment validates the concept of receptor-mediated endocytosis in the polysaccharide vesicles. DOX florescence intensity was estimated using image J software and shown in figure 8b. The biotin-tagged vesicles $V_{BIOTIN+DOX.HCl}$ showed four-fold better uptake in normal cells compared to biotin pre-treated cells. Further, this observation was validated by flow cytometry analysis (see figure 8c) with biotin pre-treated and normal HeLa cells. The results in flow cytometry plots in figure 8c showed relatively more uptake of $V_{BIOTIN+DOX.HCl}$ by HeLa cells without biotin pre-treatment. In figure 8d, the DOX internalization from $V_{DOX.HCl}$ did not show much difference between HeLa cells irrespective of their exposure to biotin pre-treatment or not. This observation was also validated by DOX intensity plot and flow cytometry data in Figures 8e and 8f. From the above discussion, it is evident that these biotin conjugated dextran vesicles can be very good candidates for targeted drug delivery in cancer cells. The cellular internalization of the foreign materials like nano-objects through endocytosis is an active transportation process and hence it is an energy-dependent process. The cellular uptake experiments at lower temperature would reduce or inactivate the endocytosis process and thereby reduce the uptake of the nano-carriers.[67-68] To evaluate the role of the temperature on the dextran nanovesicles internalisation in cells, temperature dependent cellular uptake experiment was carried out in HeLa cells at 4 °C and 37 °C. The HeLa cells were incubated with $V_{DOX.HCl}$ and $V_{BIOTIN+DOX.HCl}$ at 4º C and 37 °C for 30 minutes and subjected to imaging using confocal microscope. At 37 °C, the cellular uptake of $V_{BIOTIN+DOX.HCl}$ was two times better than $V_{DOX.HCl}$ which supported the enhancement in the endocytosis of biotin-tagged vesicles (see Figure 9b). The uptake of $V_{DOX.HCl}$ was found to be almost similar in both temperatuers indicating that the biotin free vesicles do not have impact towards the receptor mediated uptake process. The uptake of $V_{BIOTIN+DOX.HCl}$ was found to reduce almost half at 4 °C indicating that the receptor-mediated endocytosis primarily occurred under physiological temperature at 37 °C.

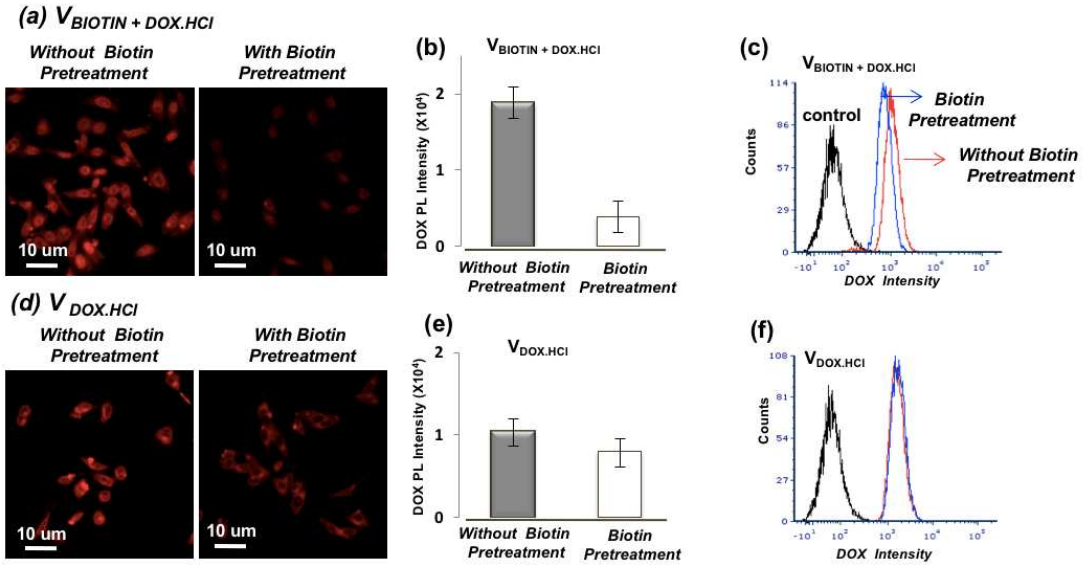

Figure 8: *(a) Confocal images showing the cellular uptake of $V_{BIOTIN+DOX.HCl,}$ in HeLa cells with or without biotin pre-treatment. (b) Corrected total cell fluorescence of DOX determined from images and plotted in bar diagram for $V_{BIOTIN+DOX.HCl}$ in HeLa cells. (c) Flow cytometry plots showing the cellular uptake of $V_{BIOTIN+ DOX.HCl}$ in HeLa cells with or without biotin pre-treatment. (d) Confocal images showing the cellular uptake of $V_{DOX.HCl,}$ in HeLa cells with or without biotin pre-treatment. (e) Corrected total cell fluorescence of DOX determined from images and plotted in bar diagram for $V_{DOX.HCl}$ in HeLa cells. (f) Flow cytometry plots showing the cellular uptake of $V_{DOX.HCl}$ in HeLa cells with or without biotin pre-treatment. For biotin pre-treatment, the cells were initially exposed to 2 mM biotin for 1h and then 2 μg/mL DOX. HCl and incubated for 4h.*

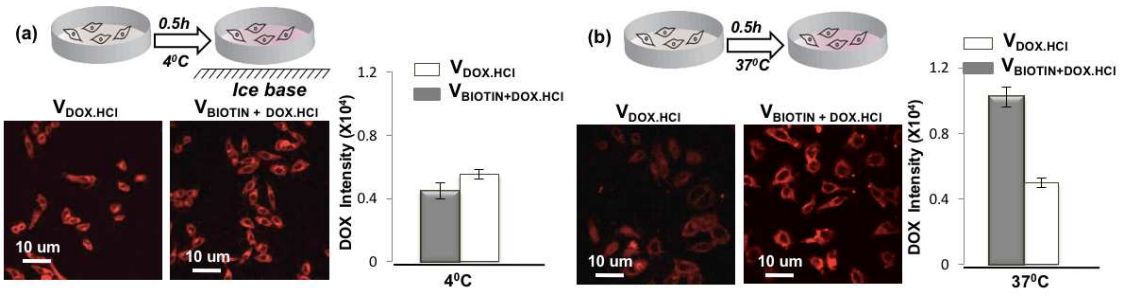

Figure 9: *(a) Cellular uptake of dextran vesicles $V_{DOX.HCl}$ and $V_{BIOTIN+DOX.HCl,}$ and the plot of corrected total cell fluorescence of DOX Intensity at 4 ºC as incubation temperature. (b) Cellular uptake of dextran vesicles $V_{DOX.HCl}$ and $V_{BIOTIN+DOX.HCl}$ and plot of corrected total cell fluorescence of DOX Intensity at 37 ºC as incubation temperature. HeLa cells are treated with 2 μg/mL of DOX concentration and incubated for 30 minutes.*

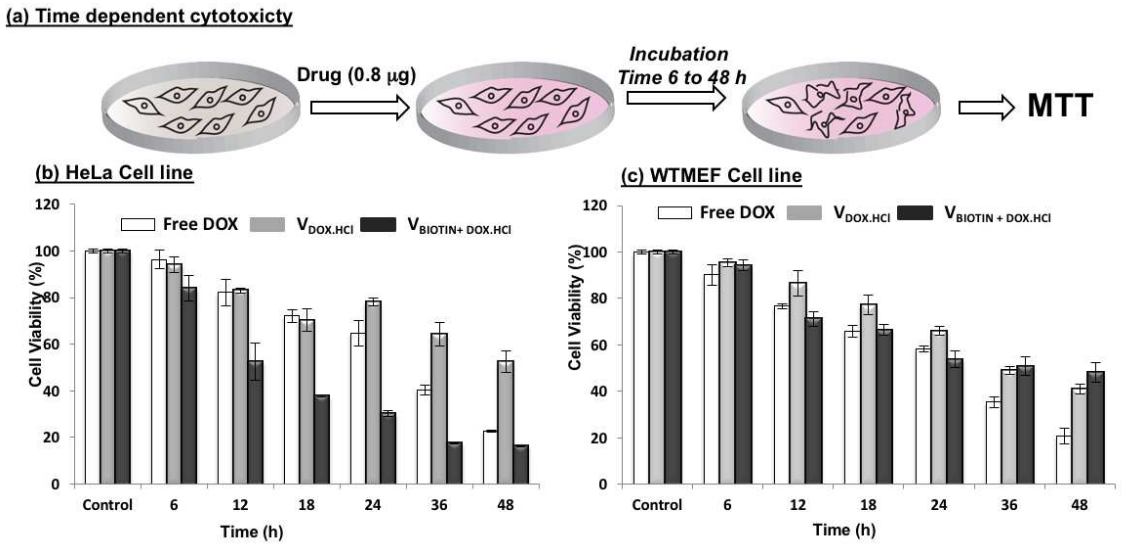

Figure 10: *(a) Schematics showing the time dependent MTT experiment. (b) Histogram showing the cytotoxicities for free DOX, $V_{DOX.HCl}$ and $V_{BIOTIN+DOX.HCl}$ in HeLa cells at various incubation time intervals. (c) Histogram showing the cytotoxicities for free DOX, $V_{DOX.HCl}$ and $V_{BIOTIN+DOX.HCl}$ in WTMEF cells at various incubation time intervals.*

The time-dependent cellular uptake studies (in Figure 6), flow cytometry analysis (in Figure 7) and the biotin pre-treatment experiment (in Figure 8) and temperature dependent endocytosis process (in Figure 9) supported the receptor-mediated drug administration in cancer cells. Since there is no significant difference between the HeLa and WT-MEF cells in terms of GSH and esterase enzyme concentration; one would anticipate similar intracellular digestion of the nano-vesicles. Thus, the difference in the cancer cell growth inhibition should arise from significant difference in their receptor-mediated drug accumulation or uptake. To validate this concept, time-dependent cytotoxicity studies were carried out for DOX concentration of 0.8 μg/ mL (based on data in Figure 5b) and subjecting the cells for MTT assay at various time intervals as shown in figure 10a. In figure 10b, the IC_{50} value (for 50 % cell killing) was attained at 12 h by biotin-tagged vesicles $V_{BIOTIN+DOX.HCl}$ in cancer (HeLa) cell. This value was thrice much faster compared to free DOX (36 h) and *and* $V_{DOX.HCl}$ (more than 48 h) in HeLa cell lines. In WT-MEF cells (see Figure 10c), the free DOX killing was much faster (< 36 h) compared to both biotin-tagged and biotin free dextran vesicles (more than 48 h). The higher uptake of the nano-carriers results in the better cell killing due to the increase in the drug concentration. This is further evident from the comparison of the time dependent MTT assay in Figure 10a and time dependent cellular uptake in figure 6. The

biotin conjugated vesicles showed enhanced uptake which further reflected on their cytotoxicity trend in suppression of cell growth in HeLa cell line. Thus the receptor-medicated endocytosis and their influence on cell growth inhibition are validated by these time dependent MTT and uptake studies. This experiment suggetsed that the biotin-tagged vesicles $V_{BIOTIN+DOX.HCl}$ provided two advantages; (i) it achieves faster rate of cell growth inhibition in cancer cells owing to its targeting ability, and (ii) it is also relatively less toxic to the WT-MEF cells. These control experiments validate the targeting ability of the biotin-tagged dextran vesicles in HeLa cell lines. In the present investigation, the approach is demonstrated exclusively for DOX.HCl delivery in HeLa cells; however, the concept is not restricted only to this example and it may be applied to large number of other cancer cells that are over expressed in biotin-receptors. Further, the dextran vesicles are capable of loading both water soluble and water insoluble drugs; thus, the approach can be in principle expanded to variety of other anticancer drugs.

Conclusion

In summary, biotin-conjugated dextran vesicles were made with multi-stimuli-responsiveness and employed them for receptor-mediated endocytosis to enhance the uptake of water soluble anticancer drug doxorubicin-hydrochloride in cancer cell lines. Renewable resource hydrophobic unit consisting of glutathione-responsive disulfide bond and enzymatic-biodegrabale aliphatic ester linkage was tailor made and conjugated along with biotin on the dextran backbone to yield amphiphilic dextran. The amphiphilic dextran self-assembled into 180 ± 20 nm vesicular nano-assemblies in aqueous medium and the size and morphology of the vesicles was characterized by dynamic light scattering, electron and atomic force microscopes. The binding ability of biotin-tagged dextran vesicle with streptavidin like receptors in the cancer cell membrane was confirmed by Avidin-HABA binding assay. The biotin-tagged vesicles showed affinity up to 25 nM towards the membrane protein indicating their excellent capability to selectively target the biotin receptors over expressed cancer cells. The dextran vesicle provided appropriate geometry to encapsulate water soluble doxorubicin-hydrochloride at the core of the vesicles. Under the intracellular stimuli such as GSH and lysosomal esterase enzymes, the vesicles ruptured to release the drug in 60 and 90 %, respectively. The combination of both GSH and esterase together accomplished 100 % drug release at the intracellular conditions. The intracellular lysosomal

degradation of these dextran vesicles was confirmed by lysosomal tracker experiments using confocal microscope. Enhanced cellular uptake of the biotin-conjugated vesicles was proven by time dependent cellular uptake studies which were validated by confocal microscopy imaging and flow cytometry analysis. Receptor mediated endocytosis mechanism was supported by control experiments such as endocytosis at lower temperature, endocytosis with biotin pre-treated cervical (HeLa) cell lines, and time dependent MTT assay and flow cytometry. All these results provide direct evidence for the targeting ability of biotin conjugated dextran vesicles in drug delivery. Based on the above observations, it can be concluded that the newly designed dextran vesicles are promising candidates for targeted delivery of anticancer drugs. Currently, the research work is focussed in this direction to explore the polysaccharide vesicles as targeted drug delivery vehicles to achieve better therapeutic efficacy in cancer.

Supporting Information: Experimental details, TGA, DSC of the polymers, plot for Avidin-HABA complex in PBS, FBS, drug release plots , ^{1}H-NMR of DEX-SS-PDP and DEX-Biotin, ^{1}H-NMR , ^{13}C-NMR , Tissue culture Conditions, drug encapsulation procedure, drug release protocol, HRMS, MALDI-TOF of compound 1 and 2 etc are provided in supporting information. This material is available free of charge via Internet at http://pubs.acs.org.

Acknowledgments: The authors thank research grant from Department of Science and Technology (DST) for the project SB/S1/OC-37/2013 Authors thank the confocal microscopy facilities at Venture Centre NCL Innovation Park Pune for all the bio-imaging experiments. Authors thanks national chemical laboratory (NCL, Pune) for HR-TEM facility. Nilesh thanks Mehak Malhotra and Sonashree Saxena for their help in Bioimaging. Nilesh U. Deshpande thanks UGC for research fellowship.

Author Information: Corresponding Author: Prof. Manickam Jayakannan [jayakannan@iiserpune.ac.in]. The authors declare no financial interest.

References

1. Ghang, Y. J.; Schramm, M. P.; Zhang, F.; Acey, R. A.; David, C. N.; Wilson, E. H.; Wang, Y.; Cheng, Q,; Hooley, R. J. Selective Cavitand-Mediated Endocytosis of Targeted Imaging Agents into Live Cells. *J. Am. Chem. Soc.* **2013** *, 135,* 7090-7093.
2. Yue, T,; Zhang,X. Cooperative Effect in Receptor-Mediated Endocytosis of Multiple Nanoparticles. *ACS Nano*, **2012**, *6*, 3196-3205.
3. Zhong, Y.; Meng, F.; Deng, C.; Zhong, Z. Ligand Directed Active Tumuor-Targeting Polymeric Nanoparticles for Cancer Therapy. *Biomacromolecules*, **2014**, *15*, 1955-1969.
4. Vacha, R.; Martinez-Veracoechea, F. J.; Frenkel, D. Receptor-Mediated Endocytosis of nanoparticles for Various Shapes. *Nano. Lett.* **2011**, *11*, 5391-5395.
5. Nguyen, D.X.; Bos, P.D.; Massague, J. Metastasis: From Disseminantion to Organ-Specific Colonization. *Nat. Rev. Cancer*, **2009**, *9*, 274-284.
6. Nie, F.; Yang, J.; Wen, S.; An, Y. L.; Ding, J.; Ju, S. H.; Zhao, Z.; Chen, H. J.; Peng, X. G.; T. C. Wong, S.; Zhao, H.; Teng, G. J. Involvement of Epidermal Growth Factor Receptor Overexpression in the Promotion of Breast Cancer Brain Metastasis. *Cancer*, **2012**, *118*, 5198-5207.
7. Neman, J.; Termini, J.; Wilczynski, S.; Vaidehi, N.; Choy, C.; Kowolik, C. M.' Li, H.; Hambrecht, A. C.; Roberts, E. Jandial, R. Human Breast Cancer Metastases To The Brain Display GABAergic Properties In The Neural Mice. *Proc. Natl. Acad. Sci.* **2014** , 111, 984-989.
8. Liu, W.; Samanta, S.K.; Smith, B. D.; Isaacs, L. Synthetic Mimics of Biotin/ (Strept) avidin. *Chem. Soc. Rev.* **2017**, *46*, 2391-2407.
9. Chen, S.; Zhao, X.; Chen, J.; Chen, J.; Kuznetsova, L.; Wong, S. S.; Ojima, I. Mechanism-Based Tumuor-Targeting Drug Delivery System. Validation of Efficient Vitamin Receptor-Mediated Endocytosis and Drug Release. *Bioconjugate. Chem.* **2010***, 21,* 979-987.
10. Yang, Z.; Lee, J. H.; Jeon, H. M.; Han. J.H.; Park, N.; He, Y.; Lee, H.; Hong, K.S.; Kang, C.; Kim, J.S. Folate-Based Near-Infrared Fluorescent Theranostic Gemcitabine Delivery. *J. Am. Chem. Soc.* **2013**,*135*, 11657-11662.

11. Barz, M.; Canal, F.; Koynov, K.; Zentel. R.; Vecent, M. J. Synthesis and InVitro Evaluation of Defined HPMA Folate Conjugates : Influence of Aggregation on Folate Receptor (FR) Mediated Cellular Uptake. *Biomacromolecules*, **2010**, *11*, 2274-2282.
12. Poh, S.; Putt, K.S.; Low, P.S. Folate-Targeted Dendrimers Selectively Accumulates at Sites of Inflammation in Mouse Models of Ulcerative Colitis and Atherosclerosis. *Biomacromolecules*, 2017, *18*, 3082-3088.
13. Zhao, F.; Yin, H.; Zhang, Z.; Li, J. Folic Acid Modified Cationic γ-Cyclodextrin-oligoethylenimine Star Polymer with Bioreducible Disulfide Linker for Efficient Targeted Gene Delivery. *Biomacromolecules*, **2013**, *14*, 476-484.
14. Zhu, Y.; Zhang, J.; Meng, F.; Deng, C.; Cheng, R.; Feijen, J.; Zhong, Z. cRGD/TAT Dual-Ligand Reversibly Cross-Linked Micelles Loaded with Docetaxel Penetrate Deeply into Tumor Tissue and Show High Antitumor Efficacy In Vivo. *ACS Appl. Mater. Interfaces.* **2017**, *9*, 35651-35663.
15. Daniels, T. R.; Bernabeu, E.; Rodriguez, J. A.; Patel. S.; Kozmann, M.; Chiapetta, D. A.; Holler, E.; Ljubimova, J. Y.; Helguera, G.; Penichet, M. L. The TranSerrin Receptor and The Targeted Delivery of Therepeutics Agents Against Cancer. *Biochimica et Biophysica Acta,* **2012**, *1820*, 291-317.
16. Sun, Q.; Qian, J.; Tian, H.; Duan, L.; Zhang, W. Rational Design of Biotinylated Probes: Fluorescent Turn-On Detection of (Strept)avidin and Bioimaging in Cancer Cells. *Chem. Comm.* **2014**, *50*, 8518-8521.
17. Ren, W. X.; Han, J.; Uhm, S.; Jang, Y. J.; Kang, C.; Kim, J. H.; Kim, J. S. Recent Development of Biotin Conjugation in Biological Imaging, Sensing, and Target Delivery. *Chem. Comm.* **2015**, *51*, 10403-10418.
18. Maiti, S.; Park, N.; Han, J. H.; Jeon, H. M.; Lee, J. H.; Bhuniya, S.; Kang, C.; Kim, J. S. Gemcitabine-Coumarin-Biotin Conjugates: A Target Specific Theranostic Anticancer Prodrug. *J. Am. Chem. Soc*. **2013**, *135*, 4567-4572.
19. Qi, K.; Ma, Q.; Remsen, E. E.; Clark, C. C.; Jr.; Wooley, K. L. Determination of the Bioavalability of Biotin Conjugated onto Shell Cross-Linked (SCK) nanoparticles. *J. Am. Chem. Soc.* **2004**, *126*, 6599-6607.
20. Wang, J. T.; Wang, L.; Ji, X.; Liu, L.; Zhao, H. Synthesis of Zwitterionic Diblock Copolymers With Clevable Biotin Groups at the Junction Points and Fabrication of

Bioconjugtes by Biotin-Streptavidin Coupling. *Macromolecules*, **2017**, *50*, 2284-2295.

21. Singh, Y.; Durga RaoViswanadham, K.K.; Jajoriya, A.K.; Meher, J.G.; Raval, K.; Jaiswal, S.; Dewangan, J.; Bora, H. K.; Rath, S. K.; Lal, J. Click Biotinylation of PLGA Template for Biotin receptor Oriented Delivery of Doxorubicin Hydrochloride in 4T1 Cell-Induced Breast Cancer. *Mol. Pharmaceutics.* **2017**, *14*, 2749-2765.
22. Pramanik, A. K.; Siddikuzzuman.; Palaniumuthu, D.; Somasundaram, K.; Samuelson, A. G. Biotin Decorated Gold Nanoparticles for Targeted Delivery of a Smart Anticancer Copper Complex: In Vitro and In Vivo Studies. *Bioconjugate. Chem.* **2016**, *27*, 2874-2885.
23. Wong Shi Kam, N.; Jessop, T. C.; Wender, P. A.; Dai, H. Nanotube Molecular Transporters: Internalisation of Carbon Nanotube-Protein Conjugates into mammalian Cells. *J. Am. Chem. Soc.* **2004**, *126*, 6850-6851.
24. Matsumura, Y.; Maeda, H. A new concept for macromolecular therapeutics in cancer chemotherapy: mechanism of tumoritropic accumulation of proteins and the antitumor agent smancs. *Cancer Res.* **1986,** *46*, 6387−6392.
25. Maeda, H. Tumor-Selective Delivery of Macromolecular Drugs via the EPR Effect: Background and Future Prospects. *Bioconjugate Chem.* **2010,** *21*, 797−802.
26. Balchandran, V. S.; Jadhav, S.R.; Vemula, K.V.; John, G. Recent Advances in Cardanol Chemistry in a Nutshell: From a Nut to Nanomaterials. *Chem. Soc. Rev.* **2013**, *42*, 427-438.
27. Ulery, B. D.; Nair, L.S.; Larencin, C. T. Biomedical Applications of Biodegradable Polymers. *J. Polym. Sci. B: Polymer Physics.* **2011**, *49*, 832-864.
28. Mizarphy, S.; Peer, D.; Polysaccharide as Building Block For Nanotherepeutics. *Chem. Soc. Rev*. **2012**, *41*, 2623-2640.
29. Basu, A.; Kunduru, K.R.; Abtew, E.; Domb, A. J. Polysaccharide-Based Conjugates for Biomedical Application. *Bioconjugate. Chem.* **2015**, *26*, 1396-1412.
30. Feng, A.; Yuan, J. Smart Nanocontainers: Progress on Novel Stimuli-Responsive Polymer Vesicles. *Macromol. Rapid. Commun.* **2014**, *35*, 767-779.
31. Wen, Y.; Oh, J. K. Recent Strategies to Develop Polysaccharide-Based Nanomaterials for Biomedical Application. *Macromol. Rapid. Commun.* **2014**, *35*, 1819-1832.

32. Allen, M. J.; Leaderach, A.; Reilly, P. J.; Mason, R. J. Polysaccharide Recognition by Surfactatnt Protein D: Novel Interactions od a C-Type Lectin With Nonterminal Glucosyl Residues. *Biochemistry.* **2001**, *40*, 7789-7798.

33. Hoai, N. T.; Sasaki, A.; Sasaki, M.; Kaga, H.; Kakuchi, T.; Satoh, T. Synthesis, Charecterusation, and Lectin Recognition pf Hyperbranched Polysaccharide Obtained From 1,6 Anhydro-D-Hexafuranose. *Biomacromolecules.* **2011,** *12*, 1891-1899.

34. Lemarchand, C.; Gref, R.; Passirani, C.; GArcion, E.; Petri, B.; Muller, R.; Constantini, D.; Couvreur, P. Influence of Polysaccharide Coating on the Interaction of Nanoparticles With Biological Systems. *Biomaterials.* **2006**, *27*, 108-118.

35. Zhang, A.; Zhang, Z.; Shi, F.; Xiao, C.; Ding, J.; Zhuang, X.; HE, C.; Chen, L.; Chen, X. Redos-Sensitive Shell-Crosslinked Polypeptide-block-Polysaccharide Micelle For Efficient Intracellular Anticancer Drug Delivery. *Macromol. Biosci.* **2013**, *13*, 1249-1258.

36. Li, Y. Z.; Liu, Z. Z.; Cheng, R.; Meng, F.; Cui, J. H.; JI, S. J.; Zhong, Z. Reversibly Stabilized Multifunctional Dextran nanoparticles Efficiently Deliver Doxorubicin Into The Nuclei of Cancer Cells. *Angew. Chem. Int. Ed.* **2009**, *48*, 9914-9918.

37. Luo, G.F.; Xu, X. D.; Zhang, J.; Yang, J.; Gong, Y.H.; Lei, Q.; Jia, H. Z.;Li, C.; Zhuo, R.X.; Zhang, X. Z. Encapsulation of an Admantane-Doxorubicin Prodrug in pH-Responsive Polysaccharide Capsule for Controlled Release. *ACS. Appl. Mater. Interfaces.* **2012**, *4*, 5317-5324.

38. Singh Chandel, A. K.; Nutan, B.; Raval,I. H.; Jewrajka, S. K. Self-Assembly of Partially Alkylated Dextran-graft-poly[(2-dimethylamino)ethyl methacrylate] Coploymer Facilitating Hydrophobic/Hydrophilic Drug Delivery and Improving Coneetwork Hydrogel Properties. *Biomacromolecules* **2018***, 19,* 1142-1153.

39. Hu, Y.; Zhao, N.; Yu, B.; Liu, F.; Xu, F. J. Versatile Types of Polysaccharide-Based Supramolecular Polycation/pDNA Nanoplexes For Gene Delivery. *Nanoscale.* **2014**, *6*, 7560-7569.

40. Tsao, C. T.; Kievit, F. M.; Ravanpay, A.; Erickson, A. E.; JEensen, M. C.; Ellnbogen, R. G.; Zhang, M. Thermoreversible Poly(ethylene glycol)-g-Chitosan Hydrogel As A Therepeutic T Lymphocyte Depot for Localized Glioblastoma Immunotherapy. *Biomacromolecules.* **2004**, *15*, 2656-2662.

41. Pramod, P. S.; Takamura, K.; Chaphekar, S.; Balasubramanian, N.; Jayakannan, M. Dextran Vesicular Carriers for Dual Encapsulation of Hydrophilic and Hydrophobic Molecules and Delivery into Cells. *Biomacromolecules* **2012**, *13*, 3627−3640.
42. Wang, S.; Wang, H.; Liu, Z.; Wang, L.; Wang, X.; Su, L.; Chang, J. Smart pH- and Reduction-Dual- Responsive Folate-PEG-Coated Polymeric Lipid Vesicles For Tumor-Triggered Targeted Drug Delivery. *Nanoscale*, **2014**, *6*, 7635-7642.
43. Wang, S.; Zhang, S.; Liu, J.; Su, L.; Wang, H.; Chang, J. pH- and Reduction Responsive Polymeric Lipid Vesicles For Enhanced Tumor Cellular Internalization and Triggered Drug Release. *ACS Appl. Mater. Interfaces.* **2014**, *6*, 10706-10713.
44. Pramod, P. S.; Shah R.; Jayakannan, M. Dual Stimuli Polysaccharide Nanovesicles for Conjugated and Physically Loaded Doxorubicin Delivery in Breast Cancer Cells. *Nanoscale*, **2015**, *7*, 6636-6652.
45. Pramod, P. S.; Deshpande, N. U.; Jayakannan, M. Real-time Drug Release Analysis of Enzyme Responsive and Cell Penetrable Polysaccharide Nano-vesicles. *J. Phys. Chem. B* **2015**, *119*, 10511-10523.
46. Pramod, P. S.; Shah R.; Chaphekar, S.; Balasubramanian, N.; Jayakannan, M. Polysaccharide Nano-vesicular Multidrug Carriers for Synergistic Killing of Cancer Cells. *Nanoscale* **2014**, *6*, 11841-11855.
47. Deshpande, N. U.; Jayakannan, M. Cisplatin-Stitched Polysaccharide Vesicles for Synergistic Cancer Therapy of Triple Antagonistic Drugs. *Biomacromolecules.* **2017**, *18*, 113-126.
48. Curcio, M.; Fernandez, B. B.; Gomez, L. D.; Concheiro, A.; Alvarez-Lorenzo, C. Hydrophobically Modified Keratin Vesicles For GSH- Responsive Intracellular Drug Release. *Bioconjugate. Chem.* **2015**, *26*, 1900-1907.
49. Saxena, S.; Jayakannan, M. Π- Conjugate Fluorophore-Tagged Enzyme-Responsive L-Amino Acid Polymer Nanocarrier and Their Color Tunable Intracellular FRET Probe in Cancer Cells. *Biomacromolecules.* **2018**, *17*, 2594-2609.
50. Aluri, R.; Jayakanna, M. Development of L-Tyrosine Based Enzyme-Responsive Amphiphilic Poly(ester-urethane) Nanocarriers For Multiple Drug Delivery To Cancer Cells. *Biomacromolecules.* **2017**, *18*, 189-200.

51. Kashyap, S.; Jayakannan, M. Amphiphilic Diblocks Sorting Into Multivesicylar Bodies and Their Fluorophore Encapsulation Capabilities. *J. Phy. Chem. B* **2012**, *116*, 9820-9831.
52. Kashyap, S.; Jayakannan, M. Thermo-Responsive and Shape TranSormable Amphiphilic Scaffold for Loading and Delivering Anticancer Drugs. *J. Mater. Chem. B* **2014**, *2*, 4142-4152.
53. Houga, C. M.; Giermanska, J.; Lecommandoux, S. B.; Borsali, R.;Taton, D.; Gnanou, Y.; Le eins, J.-F. O. Micelles and Polymersomes Obtained by Self-Assembly of Dextran and Polystyrene Based Block Copolymers. *Biomacromolecules* **2009**, *10*,32–40.
54. Burchard, W. Adv. Polym. Sci. 1983, 48, 1–124.
55. Wilhelm, S.; Anthony J.; Dai, T.Q.; Ohta, S.; Audet, J.; Dvorak,H.F.; Chan, C.W., Warren.Analysis of Nanoparticles Delivery to tumuors. *Nat. Rev. Mater*. **2016**, *1*, 1-12.
56. Ennen, F.; Boye, S.; Lederer, A.; Cernescu, M.; Komber, H.; Brutschy, B.; Voit, B.; Appelhans, D. Biohybrid Structures Consisting of Biotinylated Glycodendrimers and Proteins: Influence of the Biotin Ligand's Number and Chemical Nature on the Biotin-Avidin Conjugation. *Polym. Chem.* **2014**, *5*, 1323-1339.
57. Jia, Z.; Liu, J.; Boyer, C.; Davis, T, P.; Bulmus, V. Functional Disulfide-Stabilized Polymer-Protein Particles. *Biomacromolecules.* **2009,** *10*, 3253-3258.
58. H. I. Okur, J. Kherb and P. S. Cremer. Cations Binds Only Weakly to Amides in Aqeous Solutions. *J. Am. Chem. Soc.*, **2013**,*135*, 5062–5067.
59. Kashyap, S.; Jayakannan, M. Super LCST Thermo-Responsive Nanoparticle Assembly For ATP Binding Through The Hofmeister Effect. *J. Mater. Chem. B* **2015**,*3*, 1957-1967.
60. Sun, H.; Cheng, R.; Deng, C.; Meng, F.; Dias, A. A.; Hendriks,M.; Feijen, J.; Zhong, Z. Enzymatically and Reductively Degradable α Amino Acid- based Pol(yesteramide)s: Synthesis, Cell Compatibility and Intra cellular Anti cancer Drug Delivery. *Biomacromolecules***, 2015**, *16*, 597-605.
61. Surnar, B.; Jayakannan, M. Triple Block nanocarriers Platform For Synergistic Cancer Therapy of Antagonistics Drugs. *Biomacromolecules*, **2016**, *17*, 4075-4085.

62. Mohammad A. K.; Reineke, J. Quantitative Detection of PLGA Degradation in Tissue Following Intravenous Administration. *Mol. Pharmaceutics.* **2013**, *10*, 2183-2189.
63. Lim, J. P.; Glesson, P. A. Macropinocytosis: an Endocytic Pathway For Internalising Large Gulps. *Immunol. Cel. Biol*. **2011**, *89*, 836-843.
64. Anas, A.; Okuda, T.; Kawashima, N.; Nakayama, K.; Itoh, T.; Ishikawa, M.; Biju, V. Clatharin-Mediated Endocytosis of Quantum Dot-Peptide Conjugates in Living Cells. *ACS Nano*. **2009**, *3*, 2419-2429.
65. Lv, L.; Liu, C.; Chen, C.; Yu, X.; Chen, G,; Shi, Y.; Qin, F.; Ou, J.; Qiu, K.; Li, G. Querctin and Doxorubicin Co-Encapsulated Biotin Receptor-Targeting Nanoparticles For Minimizing Drug Resistance In Breast Cancer. *Oncotarget.* **2015**, *7*, 32184-32199.
66. Droumaguet, B. L.; Nicolas, J.; Brambilla, D.; Mura, S.; Maksimenko, A.; Kimpe, L. D.; Salvati, E.; Zona, C.; Airoldi, C.; Canovi, M.; Gobbi, M.; Noiray, M.; Ferla, B. L.; Nicotra, F.; Scheper, W.; Flore, O.; MAsserini, M.; Andrieux, K.; Couvreur, P. Versatile and Efficient Targeting Using a Single Nanoparticle Platform: Application to Cancer and Alzheimer's Disease. *ACS Nano.* **2012**, *6*, 5866-5879.
67. Zeng, X.; Zhang, Y.; Nystrom, A. Endicytic Uptake and Intracellular Trafficking of Bis-MPA-based Hyperbranched Copolymer Micelles In Breast Cancer Cells. *Biomacromolecules.* **2012**, *13*, 3814-3822.
68. Wang, H. Y.; Hua, X. W.; Jia, H. R.; Liu, P.; Gu, N.; Chen, Z.; Wu, F. G. Enhanced Cell Membrane Enrichment and Subsequent Cellular Internalization of Quantum Dots Via Cell Surface Engineering: Illuminating Plasma Membranes With Quantum Dots. *J. Mater. Chem. B.* **2016**, *4*, 834-843.

Table of Contents

Biotin-Tagged Polysaccharide Vesicular Nanocarriers for Receptor-Mediated Anticancer Drug Delivery in Cancer Cells

Nilesh Umakant Deshpande and Manickam Jayakannan*